XIII. MANGANESE NODULES: RELATIONSHIP BETWEEN COVERAGE AND ABUNDANCE IN THE NORTHERN PART OF CENTRAL PACIFIC BASIN

Keiji Handa and Katsuya Tsurusaki**

Introduction

Following observation and measurements were conducted on board in order to collect basic data for estimating nodule abundance from deep-sea photographs.

1) observation of nodule occurrence in a box corer, sizing and weighing of sampled nodules, and calculation of nodule abundance.
2) measurement of long axis, short axis, thickness, and weight of each nodule.
3) photographing deep sea floor using a one-shot camera and measurement of nodule coverage.

Procedure and equipments

Two types of box core sampler, i.e. a double spade corer and a large spade corer, were used in this cruise. Figure XI-11 (TSURUSAKI and HANDA, this cruise report) illustrates the former. It can take bottom sediments of 0.16 m^2 in area and 36 cm in depth. The latter, which is shown in Fig. XI-12, can take bottom sediments of 0.25 m^2 in area and 60 cm in depth. After the sampler was recovered onto the deck, we took photographs of the nodule occurrence on the sediment surface. Thereafter nodules were picked up to observe and measure on board as described later. Freefall grab samplers with or without a one-shot camera were also used at each station to obtain additional data of nodule samples and deep-sea photographs. They could take nodules or rocks in their hauls and small amount of sediment in their sampling tube. A one-shot camera attached inside of the sampler as shown in Fig. XIII-1 could take a picture of deep-sea floor just before sampling. Nodules sampled by freefall grab samplers were also observed and measured on board. Bottom sampling and photographing were done at 33 stations about 110 km or 1° away from each other in the GH79–1 main area, and 12 stations which were spaced over about 18 km or 10′, in the detailed survey area. Figures I-4 and I-6 show the sampling stations and Table I-6 shows the result of on-site observations.

Nodule samples were washed carefully with sea water, when they were too muddy, and were provided for following shipboard studies:

a) to determine their morphological types according to MORITANI *et al.* (1977)'s classification scheme.
b) to classify them into size fractions.
c) to weigh them in wet state using spring balances, to check the number at respective size fractions, and to calculate nodule abundance in kg/m^2.
d) to measure the length of its long axis and short axis, thickness of each nodule

*National Research Institute for Pollution and Resources, Tsukuba

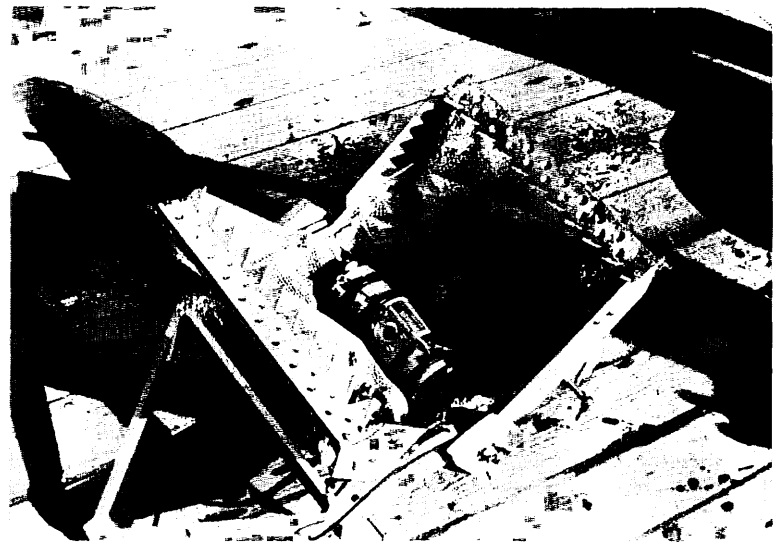

Fig. XIII-1 One-shot camera attached to inside of freefall grab sampler.

using a slide caliper, and its weight using a shipboard electrical balance (see Fig. XI-1 (TSURUSAKI and HANDA, this cruise report)).

e) to observe their internal structure on cut section.

f) to take pictures of whole nodules and cut section.

Nodule coverage in box cores and in deep-sea photographs by the one-shot camera was determined by using an optical image analyzer in the onshore laboratory after the cruise.

Results and discussion

Photographs of the top surface of the box core and deep-sea photographs are shown in Fig. XIII-2. Some photographs of the box cores are omitted because their top surface were disturbed intensively (see appendix of Chapter XI of this cruise report).

Results of observation on morphological types and size classification of sampled nodules are summarized in Appendix XII-1 (MIZUNO *et al.*, this cruise report).

Measurements of dimension and weight of each nodule were carried out at 51 sampling points (21 box cores and 30 freefall grab samples) in order to obtain quantitative relationship between nodule dimension and its weight. Some examples of the relationship between long axis and weight and the relationship between long axis and thickness are shown in Fig. XIII-3 (1–11). In these figures, morphological types of nodules are shown by respective marks, and regression lines are drawn which are obtained by the method of least squares using all measured values except those of V-type nodules. The equations for these lines are as follows:

$$W = 0.61 \times L^{2.5} \quad \text{.....(1)}$$

$$T = 0.55 \times L \quad \text{.....(2)}$$

where W: weight of nodule (gr)

T: thickness of nodule (cm)

L: length of long axis of nodule (cm)

ST. 1448 13.0°N , 178.0°W

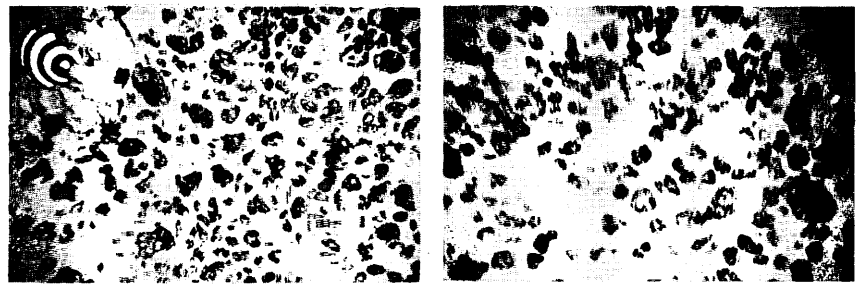

FG 115 C-1
5155 m
9.3 kg/m^2
50 %
10 cm

FG 115 C-2
5165 m
5.4 kg/m^2
35 %
10 cm

ST. 1449 13.0°N , 177.0°W

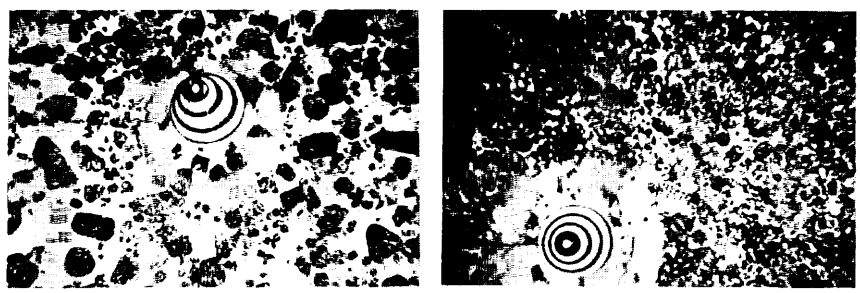

FG 116 C-1
3925 m
(0.9 kg/m^2)
50 %
10 cm

FG 116 C-2
3975 m
(0.1 kg/m^2)
75 %
10 cm

Fig. XIII-2 Top surfaces of selected box cores and deep sea photographs.

Note

1) Data accompanying each figure indicate station number, position, observation number, water depth, nodule abundance in kg/m^2, nodule coverage in %, and scale (10 cm).
2) Position of each station is rounded to 0.5° in the main survey area and to 5′ in the detailed survey area.
3) Water depth is rounded to 5 m.
4) Symbols in observation number: G(B) = double spade corer, G(B′) = large spade corer, G(B′-C) = large spade corer with one-shot camera, FG-C = freefall photo grab sampler.
5) Figures of disturbed box cores are omitted.
6) Nodule abundance in parentheses shows probably incorrect values due to imperfect sampling, judged from sea bottom photograph data by freefall photo grab sampler.

ST. 1450 13.0°N , 176.0°W

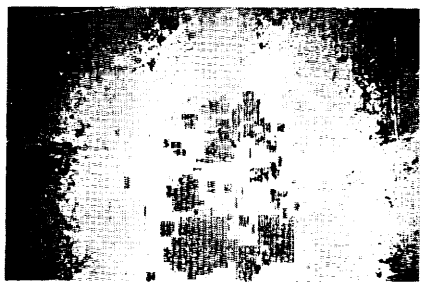

FG 117 C-1

5120 m
0 kg/m^2
0 %

10 cm

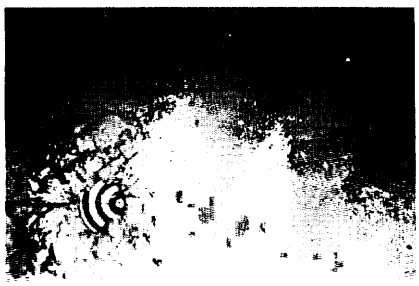

FG 117C-2

5120 m
0 kg/m^2
0 %

10 cm

ST. 1451 13.0°N , 175.0°W

G(B) 918 5500 m
trace
0 %

10 cm

FG 118 C-1

5540 m
9.9 kg/m^2
20 %

10 cm

FG 118 C-2

5485 m
8.2 kg/m^2
30 %

10 cm

ST. 1452 13.0°N , 174.0°W

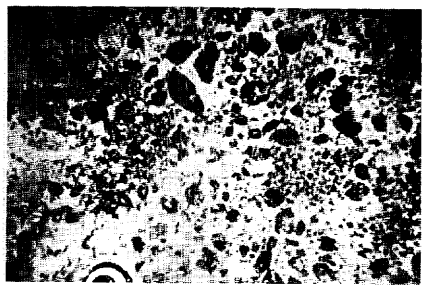

FG 119 C-1
5530 m
4.1 kg/m^2
40 %
10 cm

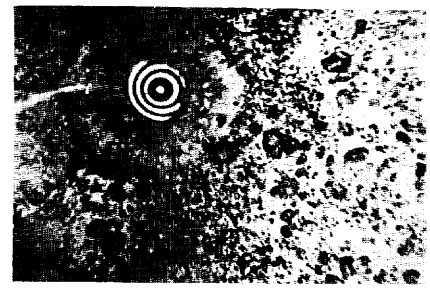

FG 119 C-2
5540 m
2.1 kg/m^2
40 %
10 cm

ST. 1453 13.0°N , 173.0°W

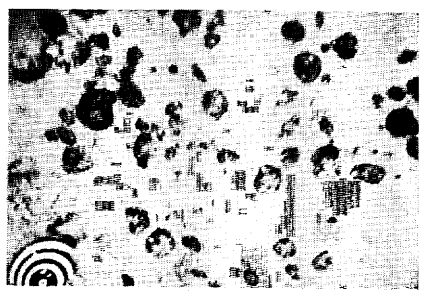

FG 120 C-1
5730 m
5.9 kg/m^2
20 %
10 cm

FG 120 C-2
5720 m
4.3 kg/m^2
20 %
10 cm

ST. 1454 12.0°N , 173.0°W

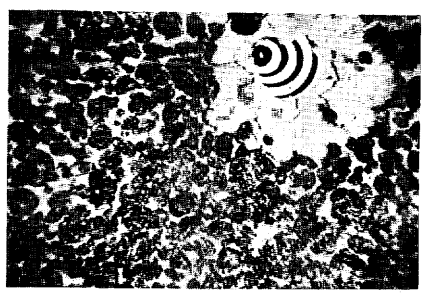

FG 121 C-1
5350 m
18.9 kg/m^2
80 %
10 cm

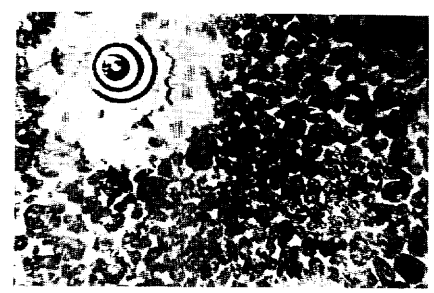

FG 121 C-2
5350 m
15.9 kg/m^2
80 %
10 cm

ST. 1455 11.0°N , 173.0°W

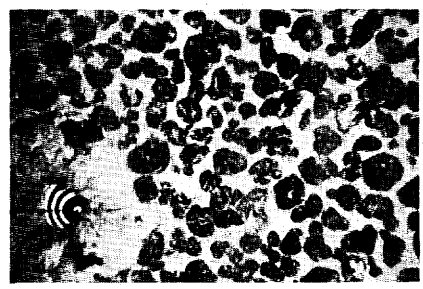

FG 122 C-1
5555 m
12.3 kg/m^2
(failed)

10 cm

FG 122 C-2
5555 m
(3.2 kg/m^2)
60 %

10 cm

ST. 1456 11.0°N , 172.0°W

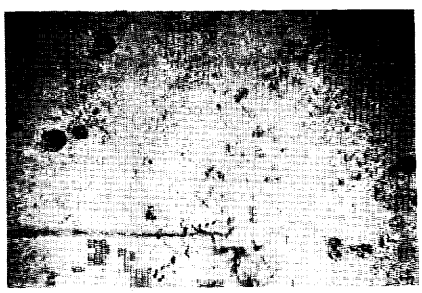

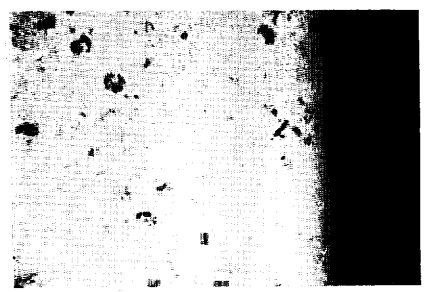

FG 123 C-1
5405 m
0.5 kg/m^2
1 %

10 cm

FG 123 C-2
5405 m
(0.2 kg/m^2)
1 %

10 cm

ST. 1457 12.0°N , 172.0°W

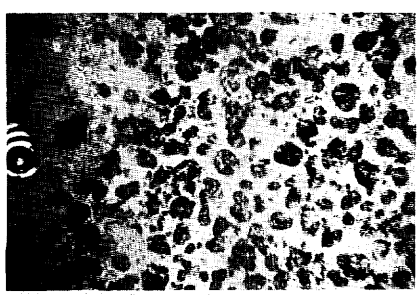

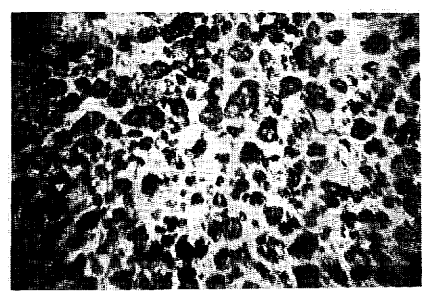

FG 124 C-1
5365 m
(0.7 kg/m^2)
50 %

10 cm

FG 124 C-2
5375 m
7.8 kg/m^2
50 %

10 cm

ST. 1458 13.0°N , 172.0°W

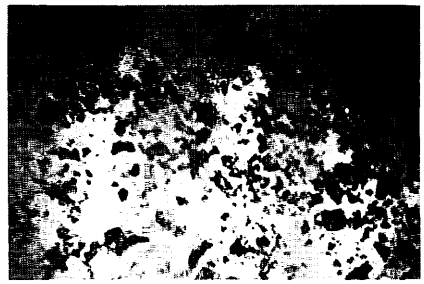

FG 125 C-1

5905 m
(trace)
35 %

10 cm

FG 125 C-2

5900 m
(0.2 kg/m^2)
(60 % : including zeolitish clay)

10 cm

ST. 1459 13.0°N , 171.0°W

G(B) 926 5630 m
11.5 kg/m^2
85 %

10 cm

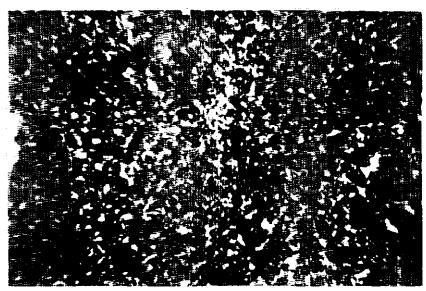

FG 126 C-1

5610 m
(5.7 kg/m^2)
85 %

10 cm

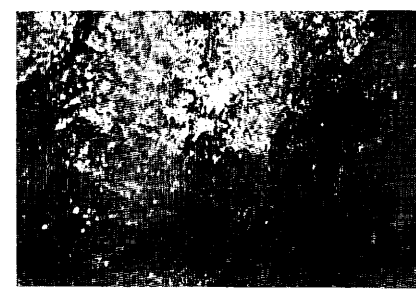

FG 126 C-2

5525 m
(outcrop ?)

ST. 1460 12.0°N , 171.0°W

G(B) 927 5185 m
12.3 kg/m^2
50 %

10 cm

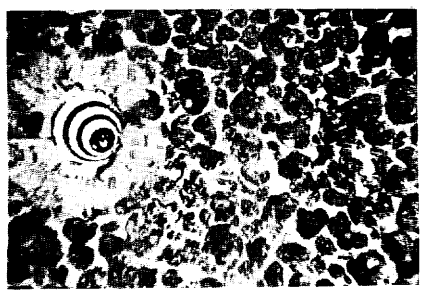

FG 127 C-1
5185 m
24.1 kg/m^2
80 %

10 cm

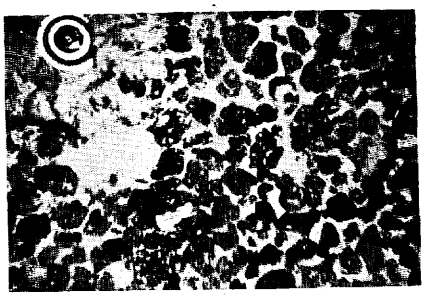

FG 127 C-2
5180 m
22.7 kg/m^2
80 %

10 cm

ST. 1461 11.0°N , 171.0°W

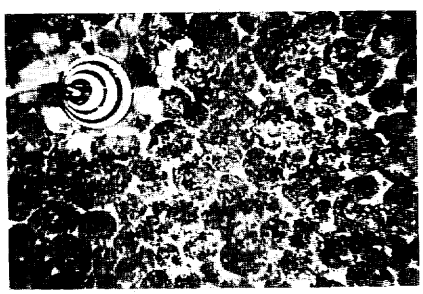

FG 128 C-1
5515 m
33.9 kg/m^2
85 %

10 cm

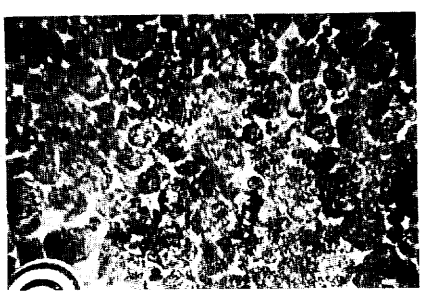

FG 128 C-2
5505 m
(7.8 kg/m^2)
85 %

10 cm

ST. 1462 11.5°N , 170.0°W

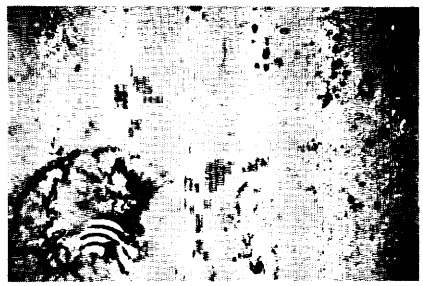

FG 129 C-1
4850 m
0.2 kg/m^2
1 %
10 cm

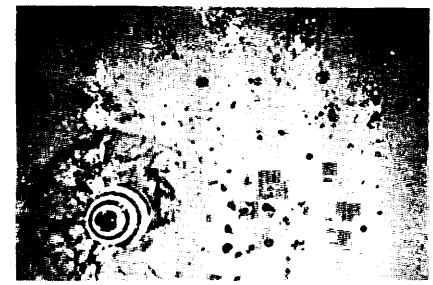

FG 129 C-2
4855 m
trace
3 %
10 cm

ST. 1463 12.0°N , 170.0°W

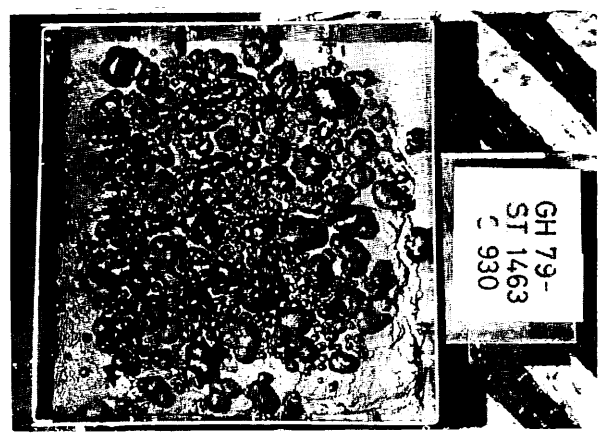

G(B) 930 5765 m
13.6 kg/m^2
75 %
10 cm

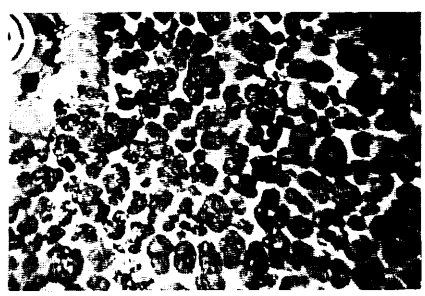

FG 130 C-1
5745 m
19.1 kg/m^2
75 %
10 cm

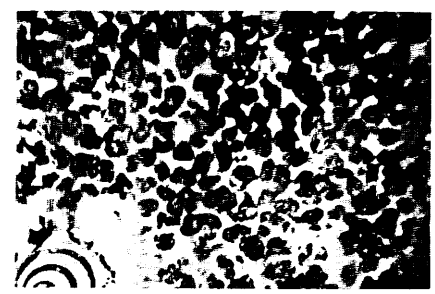

FG 130 C-2
5750 m
21.9 kg/m^2
75 %
10 cm

ST. 1464 13.0°N , 170.0°W

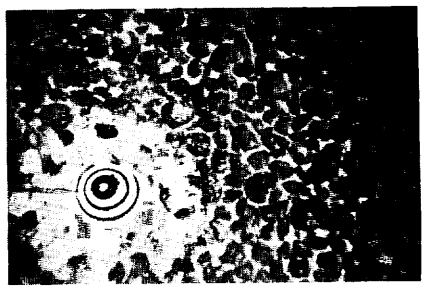

FG 131 C-1
5775 m
16.0 kg/m^2
85 %

10 cm

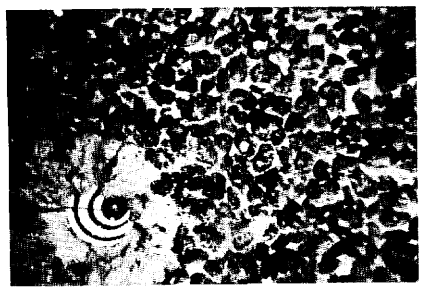

FG 131 C-2
5775 m
13.8 kg/m^2
85 %

10 cm

ST. 1465 13.0°N , 169.0°W

FG 132 C-1
5240 m
(0.2 kg/m^2)
80 %

10 cm

FG 132 C-2
5170 m
(3.1 kg/m^2)
80 %

10 cm

ST. 1466 12.0°N , 169.0°W

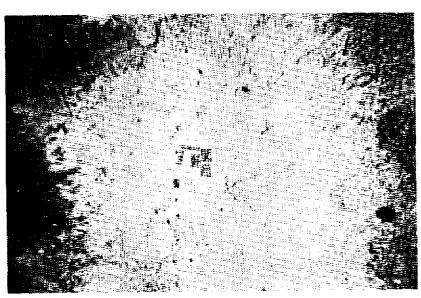

FG 133 C-1
5445 m
0.1 kg/m^2
0 %

10 cm

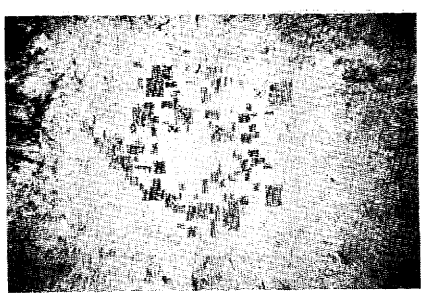

FG 133 C-2
5440 m
trace
0 %

10 cm

ST. 1467 11.0°N , 169.0°W

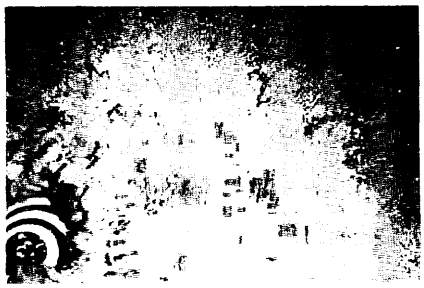

FG 134 C-1
5225 m
0 kg/m^2
0 %

10 cm

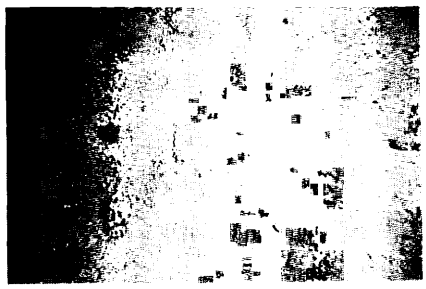

FG 134 C-2
5225 m
trace
0 %

10 cm

ST. 1468 11.0°N , 168.0°W

FG 135 C-1
5305 m
2.1 kg/m^2
5 %

10 cm

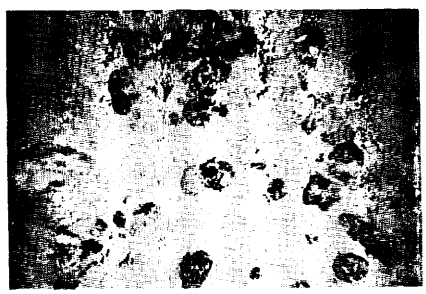

FG 135 C-2
5320 m
6.6 kg/m^2
15 %

10 cm

ST. 1469 12.0°N , 168.0°W

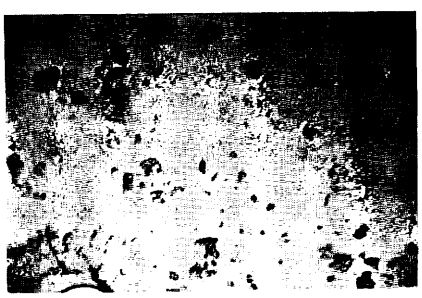

FG 136 C-1
5355 m
trace
5 %

10 cm

FG 136 C-2
5360 m
trace
0 %

10 cm

ST. 1470 13.0°N , 168.0°W

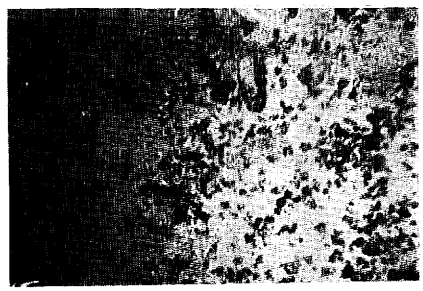

FG 137 C-1
5485 m
6.2 kg/m^2
(failed)

FG 137 C-2
5525 m
(0.4 kg/m^2)
25 %

10 cm

ST. 1471 13.0°N , 167.0°W

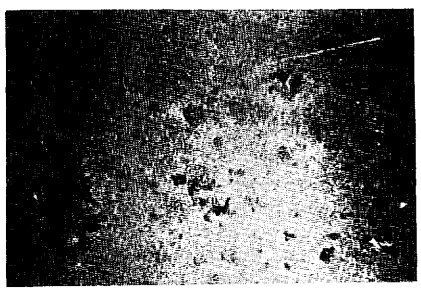

FG 138 C-1
5205 m
trace
0 %

10 cm

FG 138 C-2
5245 m
0.2 kg/m^2
0 %

10 cm

ST. 1472 12.0°N , 167.0°W

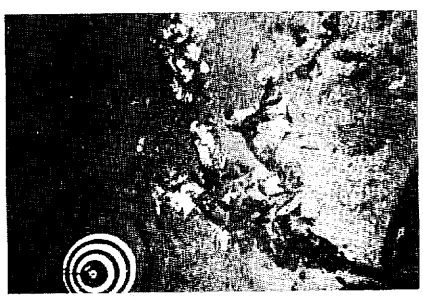

FG 139 C-1
5370 m
0 kg/m^2
(30 % : including
zeolite concretion)

10 cm

FG 139 C-2
5410 m
2.6 kg/m^2
55 %

10 cm

ST. 1473 11.5°N , 167.0°W

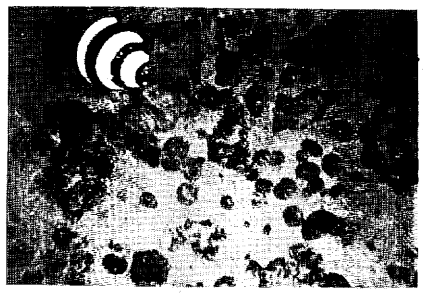

FG 140 C-1
4985 m
7.5 kg/m^2
45 %

10 cm

FG 140 C-2
4985 m
(1.0 kg/m^2)
50 %

10 cm

ST. 1474 10°10'N , 167°20'W

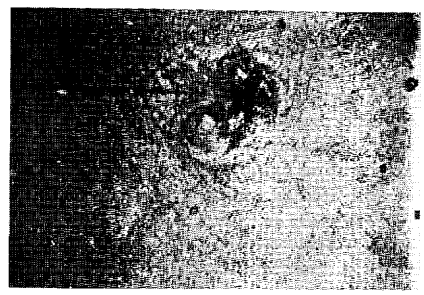

FG 141 C-1
5180 m
0 kg/m^2
0 %

10 cm

FG 141C-2
5155 m
0 kg/m^2
(failed)

ST. 1475 10°00'N , 167°20'W

FG 142 C-1
5200 m
0.1 kg/m^2
0 %

10 cm

FG 142 C-2
5200 m
0 kg/m^2
0 %

10 cm

ST. 1476 9°50'N , 167°20'W

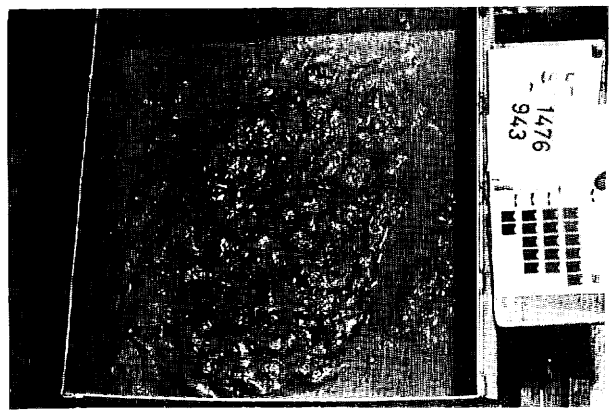

G(B') 943 5150 m
0.2 kg/m^2
<1 %

10 cm

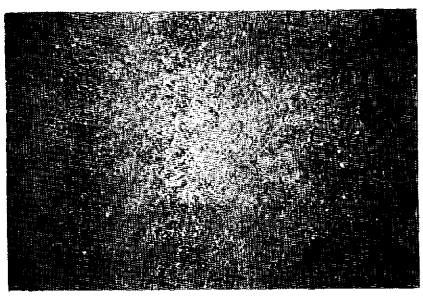

FG 143 C-1
5160 m
trace
0 %

10 cm

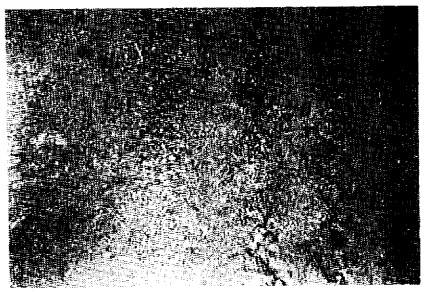

FG 143 C-2
5160 m
0.9 kg/m^2
<1 %

10 cm

ST. 1478 10°00'N , 167°30'W

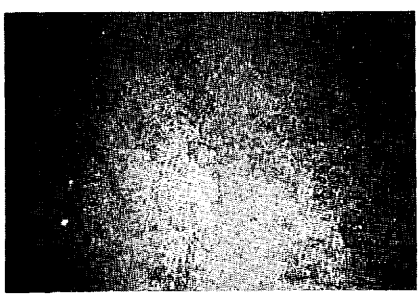

FG 145 C-1
5225 m
(failed)
0 %

10 cm

FG 145 C-2
5220 m
0 kg/m^2
0 %

10 cm

ST. 1477 9°50'N , 167°35'W

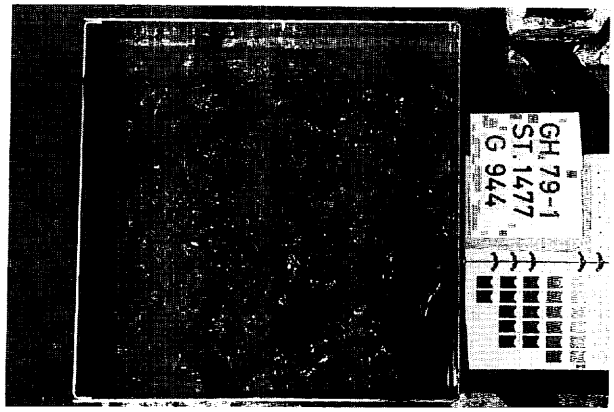

G(B) 944 5200 m
0.5 kg/m^2
1 %

10 cm

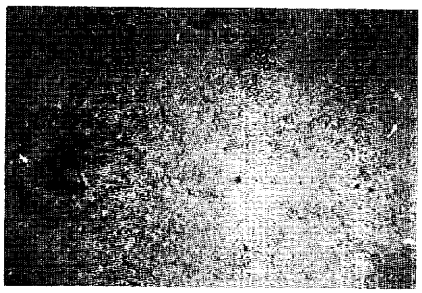

FG 144 C-1
5210 m
0 kg/m^2
0 %

10 cm

FG 144 C-2
5205 m
2.7 kg/m^2
5 %

10 cm

ST. 1479 10°10'N , 167°30'W

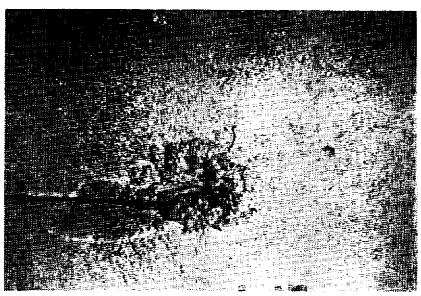

FG 146 C-1
5260 m
0 kg/m^2
0 %

10 cm

FG 146 C-2
5260 m
0 kg/m^2
(failed)

10 cm

ST. 1480 10°10'N , 167°50'W

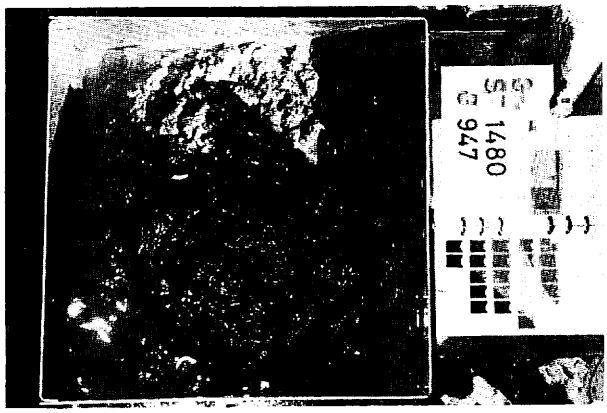

G(B) 947 5255 m
2.3 kg/m^2
3 %

10 cm

FG 147 C-1
5255 m
8.1 kg/m^2
15 %

10 cm

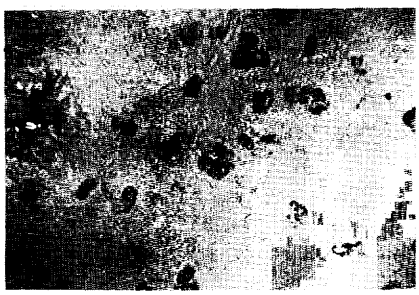

FG 147 C-2
5250 m
4.3 kg/m^2
15 %

10 cm

ST. 1482 9°50'N , 167°50'W

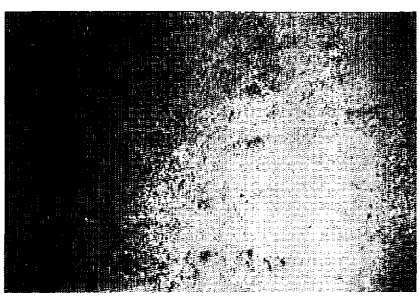

FG 149 C-2
5220 m
0.6 kg/m^2
0 %

10 cm

ST. 1481 10°00'N , 167°50'W

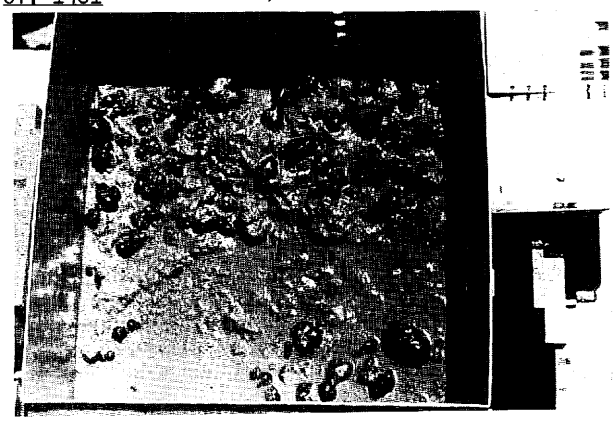

G(B'-C) 948 5285 m
12.2 kg/m^2
60 %

10 cm

FG 148 C-1
5290 m
18.0 kg/m^2
60 %

10 cm

FG 148 C-2
5290 m
12.6 kg/m^2
60 %

10 cm

ST. 1483 9°50'N , 167°40'W

G(B) 950 5210 m
2.1 kg/m^2
5 %

10 cm

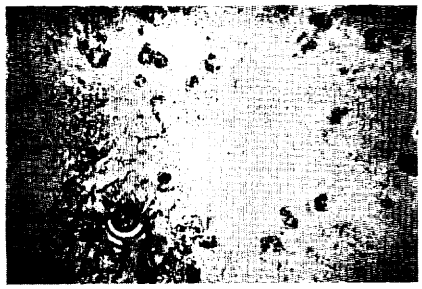

FG 150 C-1

5210 m
3.9 kg/m^2
5 %

10 cm

FG 150 C-2

5210 m
(1.1 kg/m^2)
(failed)

ST. 1484 10°00'N , 167°40'W

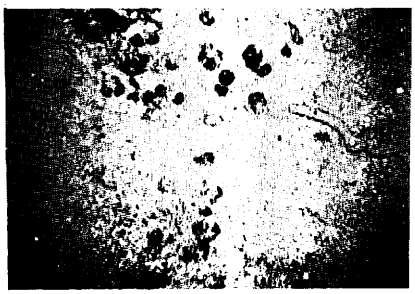

G(B'-C) 951

5245 m
1.8 kg/m^2
5 %

10 cm

10 cm

5 %

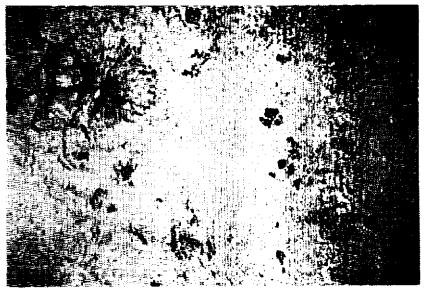

FG 151 C-1

5250 m
3.6 kg/m^2
3 %

10 cm

FG 151 C-2

5250 m
3.3 kg/m^2
3 %

10 cm

ST. 1485 10°10'N , 167°40'W

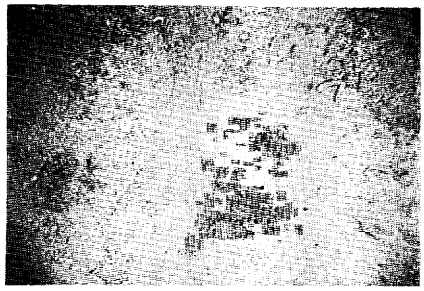

FG 152 C-1
5260 m
0 kg/m^2
0 %
10 cm

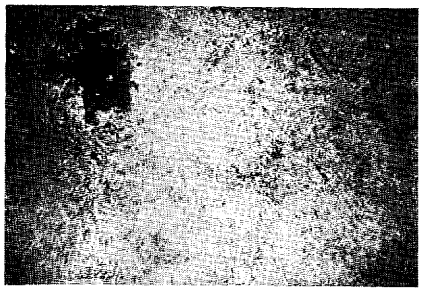

FG 152 C-2
5260 m
0 kg/m^2
0 %
10 cm

ST. 1481A 10°00'N , 167°50'W

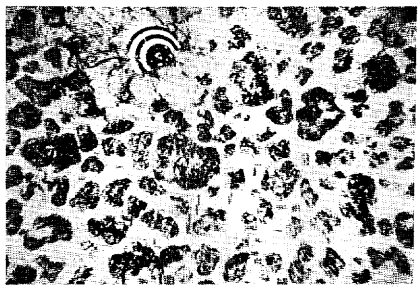

FG 153 C-1
5285 m
18.9 kg/m^2
55 %
10 cm

FG 153 C-2
5290 m
19.3 kg/m^2
55 %
10 cm

ST. 1481A 10°00'N , 167°50'W

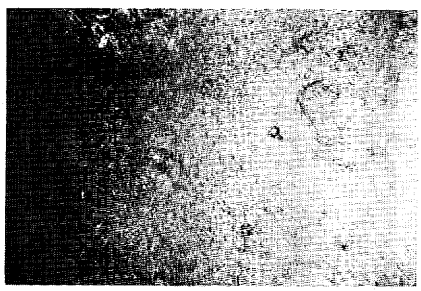

FG 153 C-3
5290 m
0 kg/m^2
0 %
10 cm

FG 153 C-4
5290 m
11.6 kg/m^2
45 %
10 cm

ST. 1481A-1 – ST. 1484A

freefall photo grab samplers deployments
10°00'N , 167°50'W through 10°00'N , 167°40'

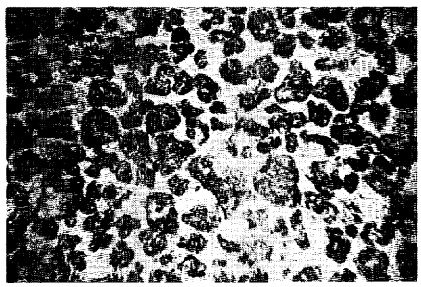

FG 154 C-1

5300 m
17.6 kg/m^2
70 %

10 cm

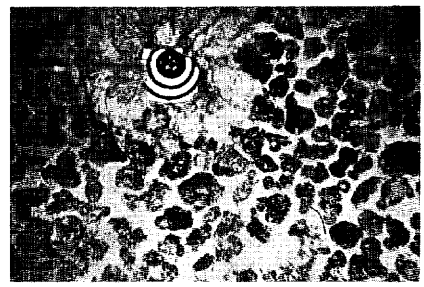

FG 154 C-2

5295 m
17.7 kg/m^2
70 %

10 cm

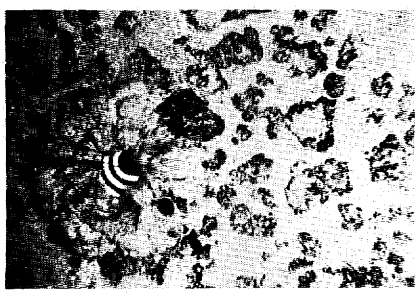

FG 154 C-3

5300 m
9.2 kg/m^2
50 %

10 cm

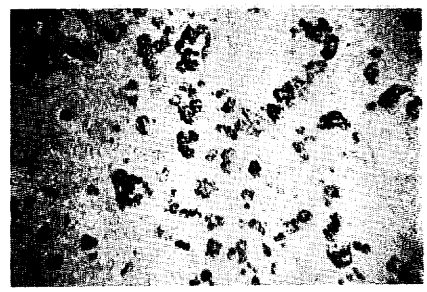

FG 154 C-4

5285 m
(1.1 kg/m^2)
20 %

10 cm

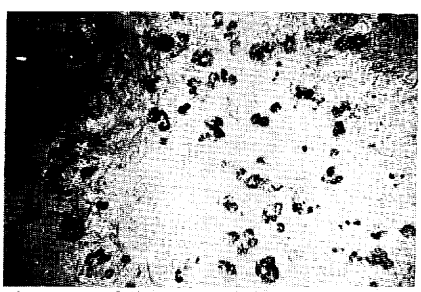

FG 154 C-5

5275 m
(7.6 kg/m^2)
15 %

10 cm

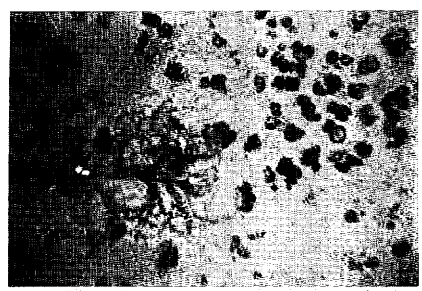

FG 154 C-6

5255 m
7.3 kg/m^2
25 %

10 cm

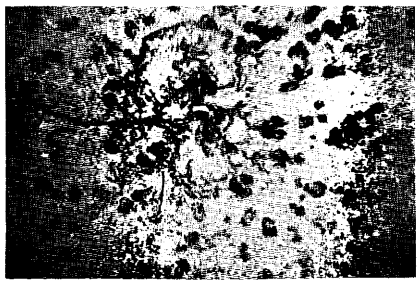

FG 154 C-7

5245 m
6.6 kg/m^2
15 %

10 cm

FG 154 C-8

5250 m
3.2 kg/m^2
5 %

10 cm

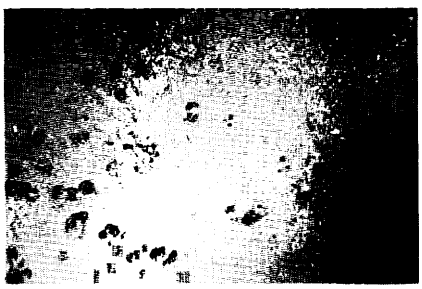

FG 154 C-9

5255 m
2.9 kg/m^2
10 %

10 cm

FG 154 C-10

5250 m
1.9 kg/m^2
0 %

10 cm

ST. 1484A-1 – ST. 1478A

freefall photo grab samplers deployments
10°00'N , 167°40'W through 10°00'N , 167°30'W

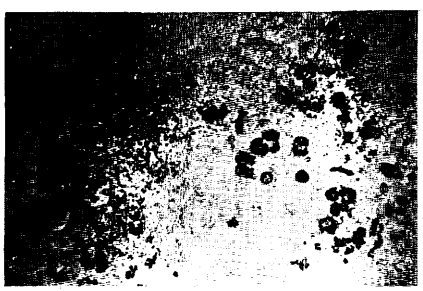

FG 155 C-1

5250 m
3.6 kg/m^2
10 %

10 cm

FG 155 C-2

5250 m
3.5 kg/m^2
10 %

10 cm

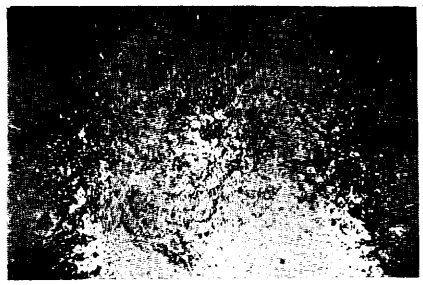

FG 155 C-3
5240 m
0.5 kg/m^2
0 %

10 cm

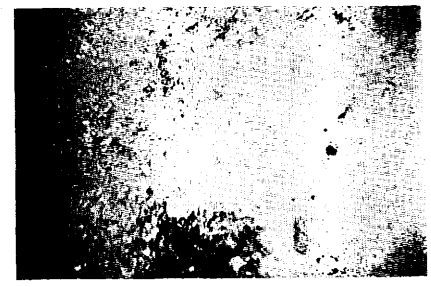

FG 155 C-4
5235 m
trace
0 %

10 cm

FG 155 C-5
5230 m
0 kg/m^2
0 %

10 cm

FG 155 C-6
5230 m
0 kg/m^2
0 %

10 cm

FG 155 C-7
5225 m
trace
0 %

10 cm

FG 155 C-8
5225 m
0 kg/m^2
0 %

10 cm

FG 155 C-9

5220 m
0 kg/m^2
0 %

10 cm

ST. 1481A-2 10°00'N , 167°50'W

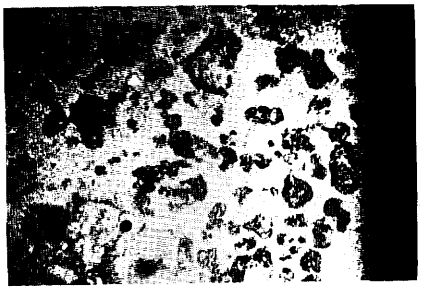

FG 156 C-1

5295 m
(0.6 kg/m^2)
40 %

10 cm

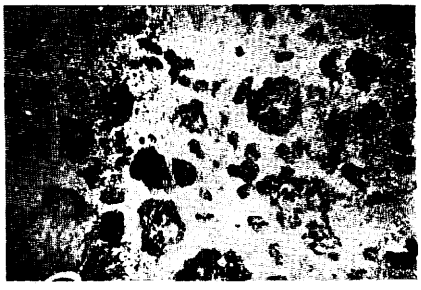

FG 156 C-2

5290 m
(trace)
40 %

10 cm

ST. 1481A-2 10°00'N , 167°50'W

FG 156 C-4

5270 m
6.0 kg/m^2
30 %

10 cm

ST. 1486 10°35'N , 168°00'W

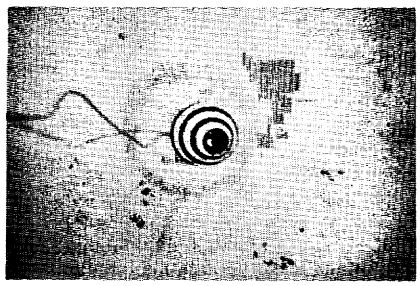

FG 157 C

1900 m
0 kg/m^2
0 %

10 cm

ST. 1452A 13.0°N , 174.0°W

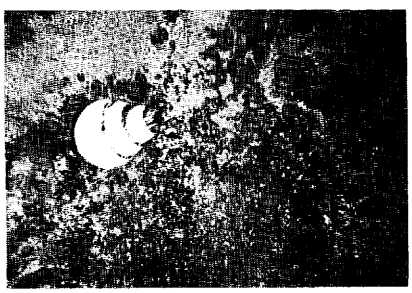

FG 158 C-1

5590 m
(0.2 kg/m^2)
75 %

10 cm

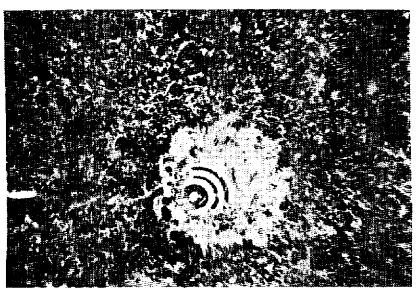

FG 158 C-2

5565 m
4.0 kg/m^2
(90 % : including pebbles of rock)

10 cm

ST. 1487 12.0°N , 174.0°W

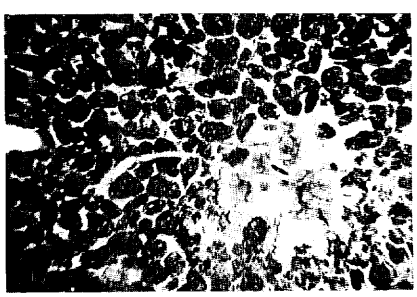

FG 159 C-1

5610 m
15.9 kg/m^2
75 %

10 cm

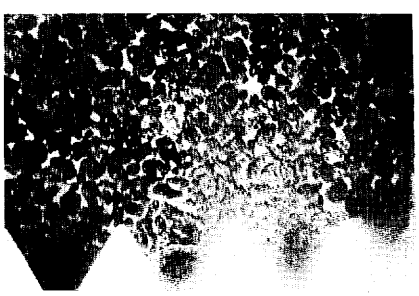

FG 159 C-2

5615 m
19.0 kg/m^2
90 %

10 cm

ST. 1488 11.0°N , 174.0°W

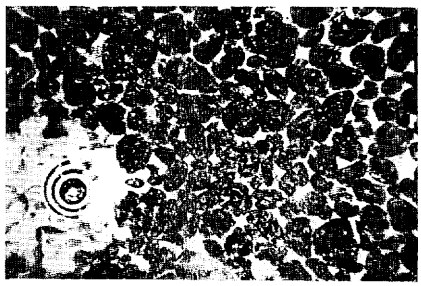

FG 160 C-1

5535 m
17.6 kg/m^2
80 %

10 cm

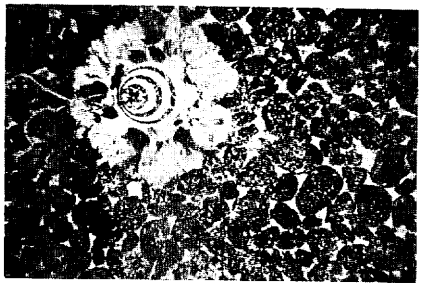

FG 160 C-2

5540 m
23.7 kg/m^2
80 %

10 cm

ST. 1489 12.0°N , 175.0°W

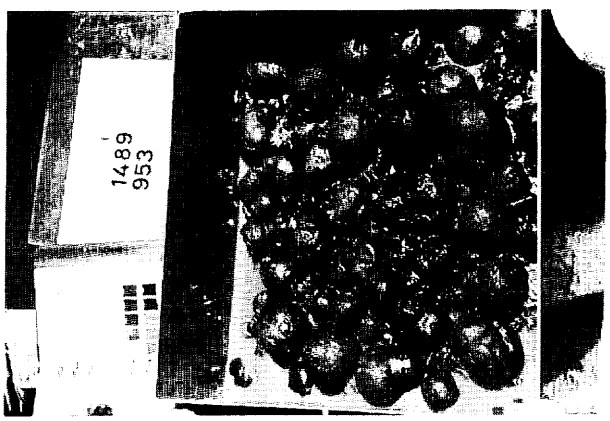

G(B) 953

5370 m
43.8 kg/m^2
80 %

10 cm

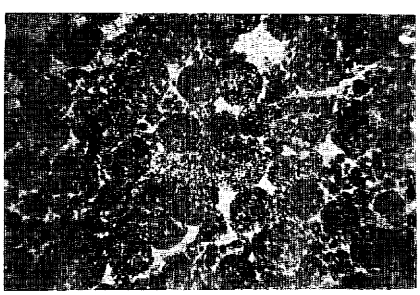

FG 161 C-1

5385 m
(0 kg/m^2)
80 %

10 cm

FG 161 C-2

5360 m
(0 kg/m^2)
(failed)

10 cm

ST. 1490 12.0°N , 176.0°W

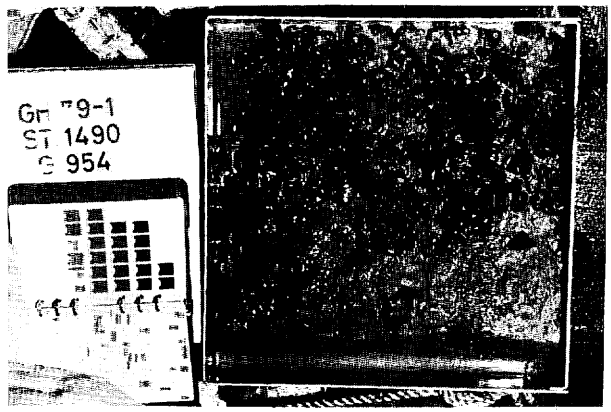

G(B) 954 4875 m
9.9 kg/m^2
75 %

10 cm

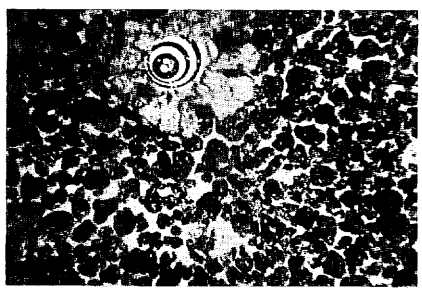

FG 162 C-1
4855 m
15.7 kg/m^2
75 %

10 cm

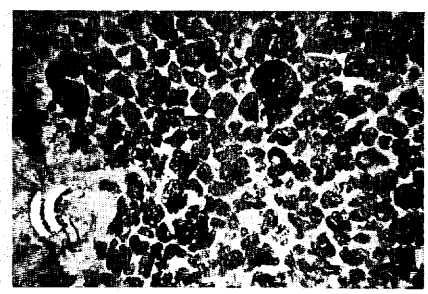

FG 162 C-2
4865 m
(8.9 kg/m^2)
75 %

10 cm

ST. 1492 12.0°N , 178.0°W

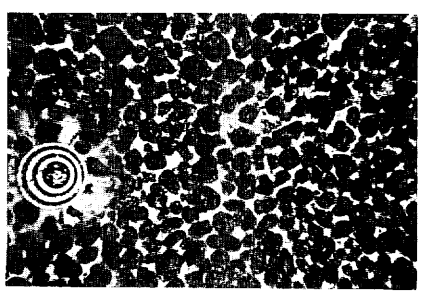

FG 164 C-1
4225 m
(7.2 kg/m^2)
80 %

10 cm

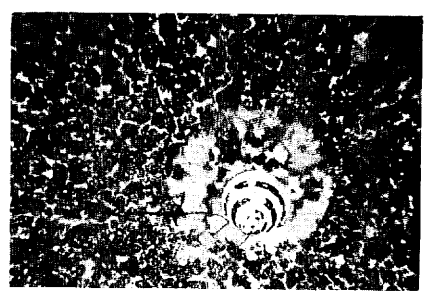

FG 164 C-2
4225 m
(2.2 kg/m^2)
90 %

10 cm

ST. 1491 12.0°N , 177.0°W

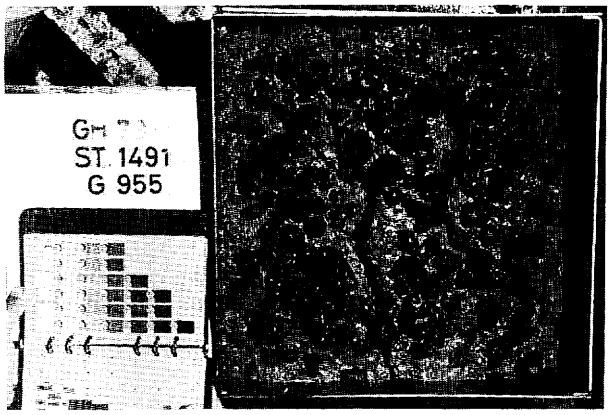

G(B) 955 4515 m
10.0 kg/m^2
75 %

10 cm

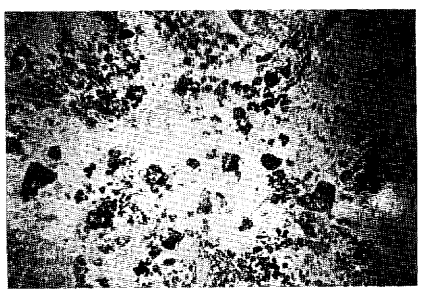

FG 163 C-1
4565 m
(0.0 kg/m^2)
35 %

10 cm

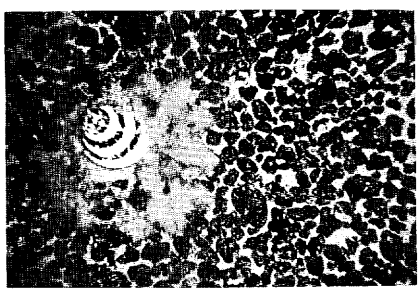

FG 163 C-2
4530 m
(1.2 kg/m^2)
75 %

10 cm

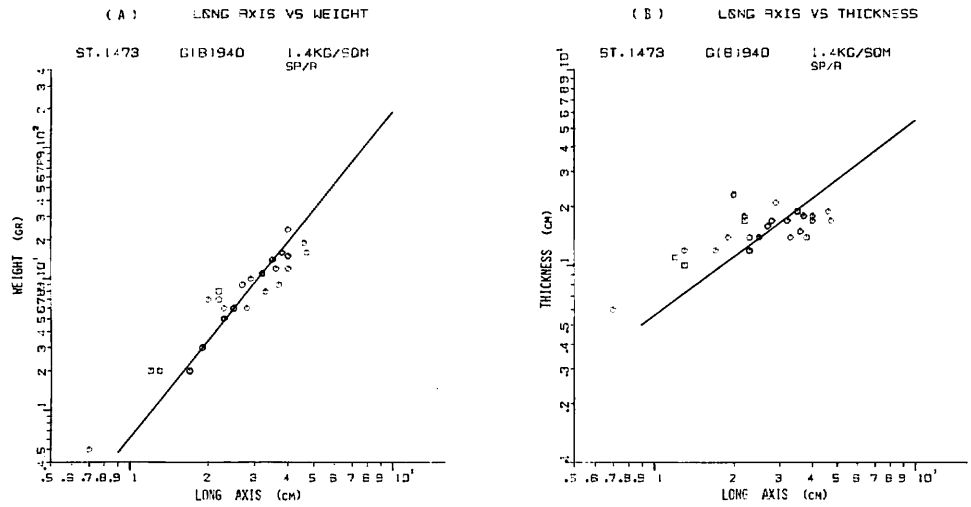

(1)

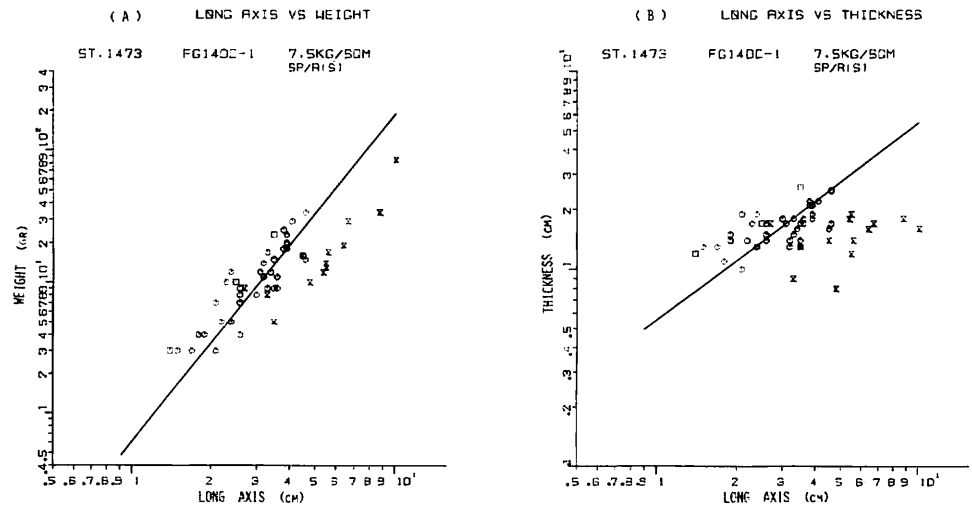

(2)

Fig. XIII-3 (1–11) (A) Relationship between long axis and weight of nodule, (B) Relationship between long axis and thickness of nodule.

(note) morphological types of manganese nodules. ( ): symbols used in Figures.

- □ Sr (S/R)
- ⊙ SPr (SP/R)
- △ SEr (SE/R)
- + DPr (DP/R)
- × Dr (D/R)
- ◇ Db (D/B)
- ⧖ V
- ↟ Ss (S/S)
- ⧖ SPs (SP/S)
- Z Ds (D/S)
- Y DPs (DP/S)
- ⌑ ISs (IS/S)
- ✳ IDPs (IDP/S)

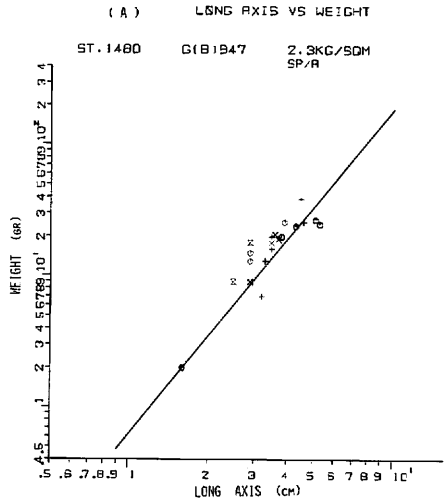
(A)
LONG AXIS VS WEIGHT
ST.1480 G(B)1947 2.3KG/SQM
SP/R
WEIGHT (GR)
LONG AXIS (CM)

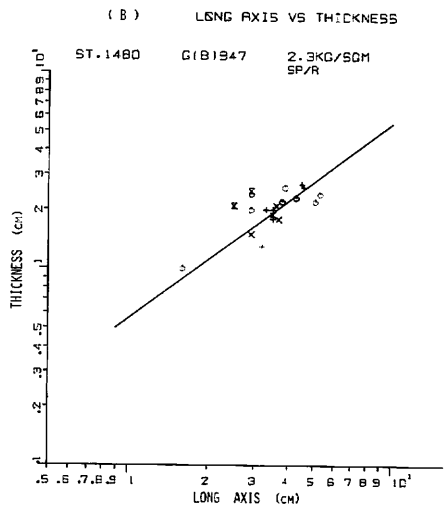
(B)
LONG AXIS VS THICKNESS
ST.1480 G(B)1947 2.3KG/SQM
SP/R
THICKNESS (CM)
LONG AXIS (CM)

(3)

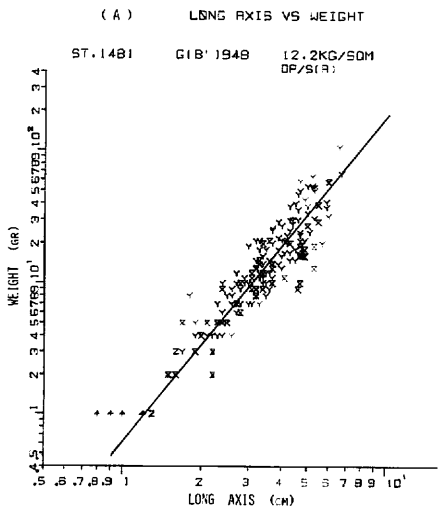
(A)
LONG AXIS VS WEIGHT
ST.1481 G(B')1948 12.2KG/SQM
DP/S(R)
WEIGHT (GR)
LONG AXIS (CM)

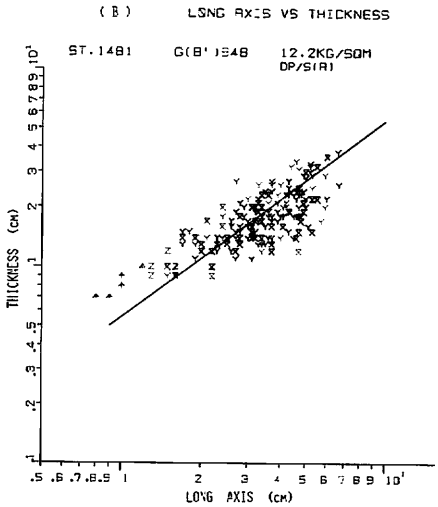
(B)
LONG AXIS VS THICKNESS
ST.1481 G(B')1948 12.2KG/SQM
DP/S(R)
THICKNESS (CM)
LONG AXIS (CM)

(4)

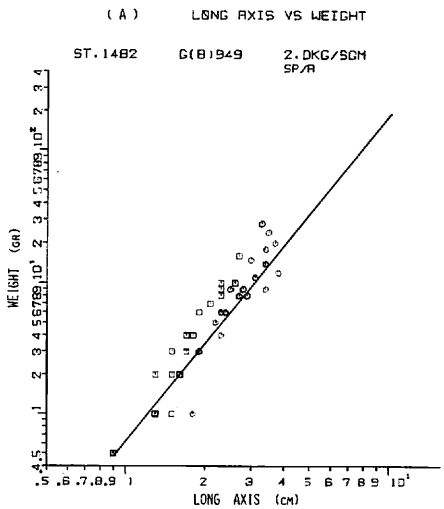
(A)
LONG AXIS VS WEIGHT
ST.1482 G(B)1949 2.0KG/SQM
SP/R
WEIGHT (GR)
LONG AXIS (CM)

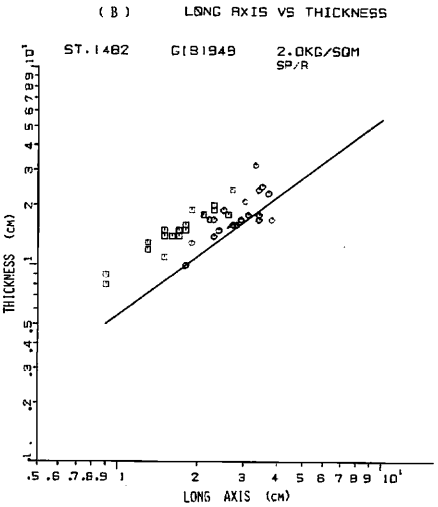
(B)
LONG AXIS VS THICKNESS
ST.1482 G(B)1949 2.0KG/SQM
SP/R
THICKNESS (CM)
LONG AXIS (CM)

(5)

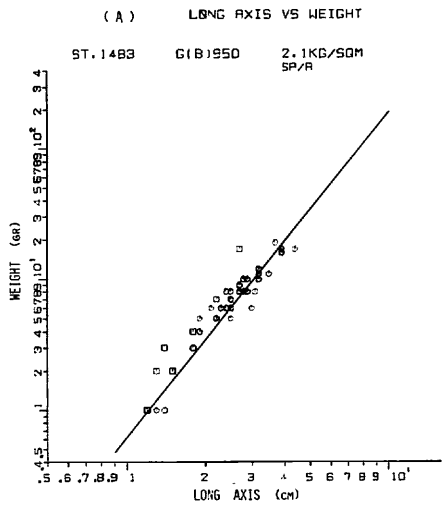
(A) LONG AXIS VS WEIGHT
ST.1483 G(B)950 2.1KG/SQM
SP/R
WEIGHT (GR)
LONG AXIS (CM)

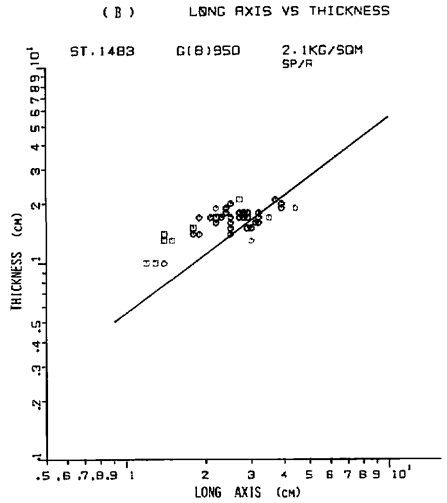
(B) LONG AXIS VS THICKNESS
ST.1483 G(B)950 2.1KG/SQM
SP/R
THICKNESS (CM)
LONG AXIS (CM)

(6)

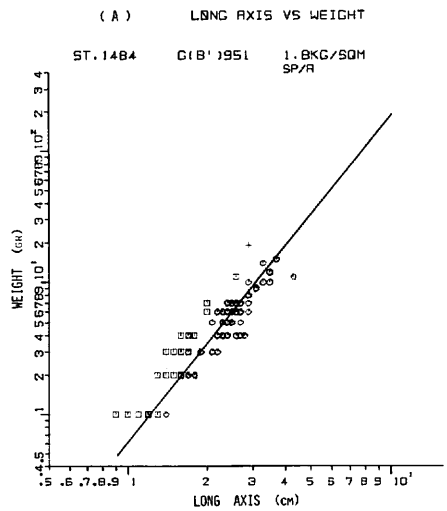
(A) LONG AXIS VS WEIGHT
ST.1484 G(B')951 1.8KG/SQM
SP/R
WEIGHT (GR)
LONG AXIS (CM)

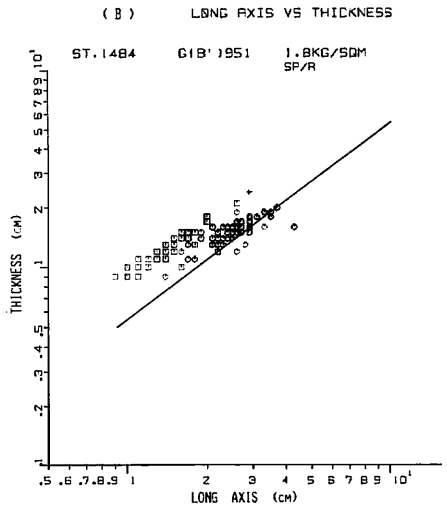
(B) LONG AXIS VS THICKNESS
ST.1484 G(B')951 1.8KG/SQM
SP/R
THICKNESS (CM)
LONG AXIS (CM)

(7)

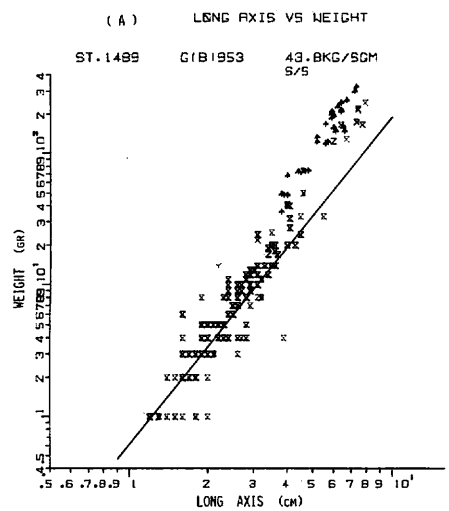
(A) LONG AXIS VS WEIGHT
ST.1489 G(B)953 43.8KG/SQM
S/S
WEIGHT (GR)
LONG AXIS (CM)

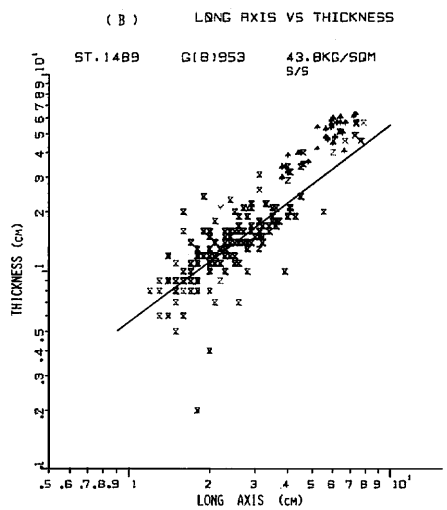
(B) LONG AXIS VS THICKNESS
ST.1489 G(B)953 43.8KG/SQM
S/S
THICKNESS (CM)
LONG AXIS (CM)

(8)

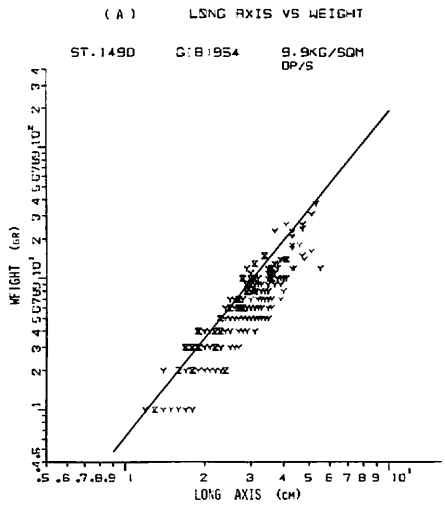
(A) LONG AXIS VS WEIGHT
ST.1490 GIB1954 9.9KG/SQM
DP/S
WEIGHT (GR)
LONG AXIS (CM)

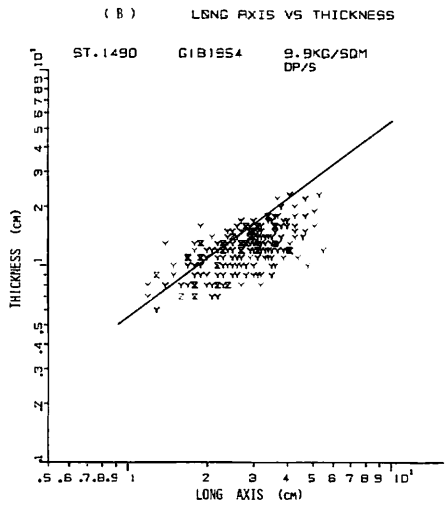
(B) LONG AXIS VS THICKNESS
ST.1490 GIB1954 9.9KG/SQM
DP/S
THICKNESS (CM)
LONG AXIS (CM)

(9)

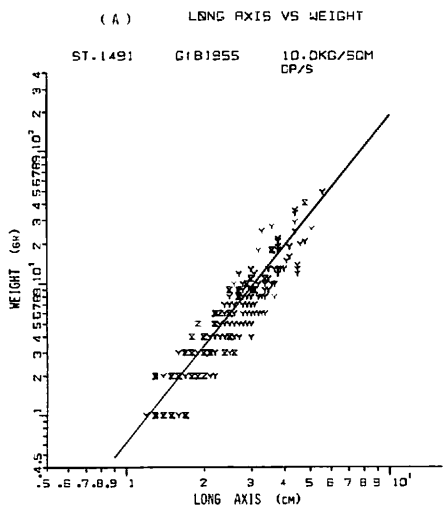
(A) LONG AXIS VS WEIGHT
ST.1491 GIB1955 10.0KG/SQM
DP/S
WEIGHT (GR)
LONG AXIS (CM)

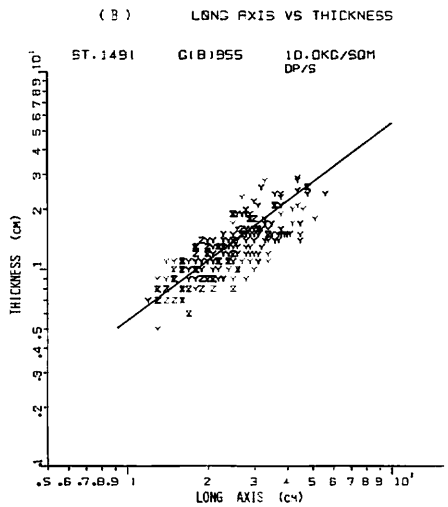
(B) LONG AXIS VS THICKNESS
ST.1491 GIB1955 10.0KG/SQM
DP/S
THICKNESS (CM)
LONG AXIS (CM)

(10)

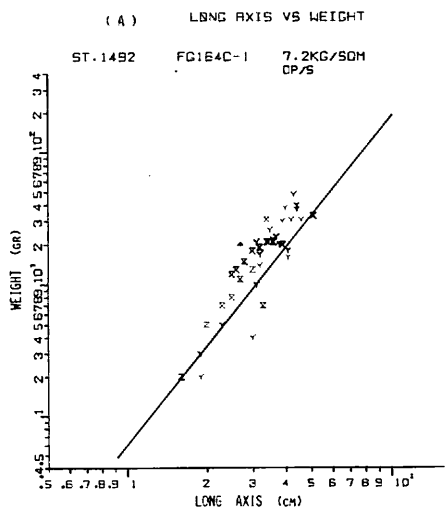
(A) LONG AXIS VS WEIGHT
ST.1492 FG164C-1 7.2KG/SQM
DP/S
WEIGHT (GR)
LONG AXIS (CM)

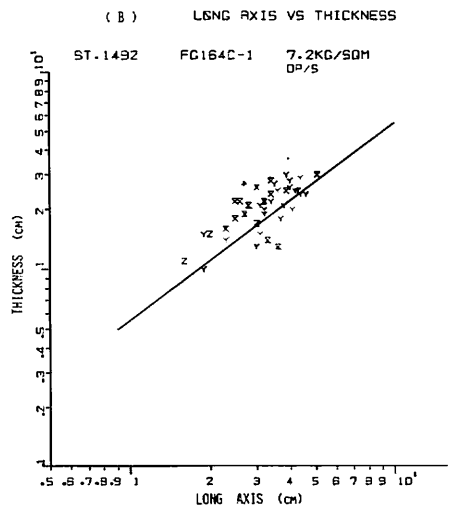
(B) LONG AXIS VS THICKNESS
ST.1492 FG164C-1 7.2KG/SQM
DP/S
THICKNESS (CM)
LONG AXIS (CM)

(11)

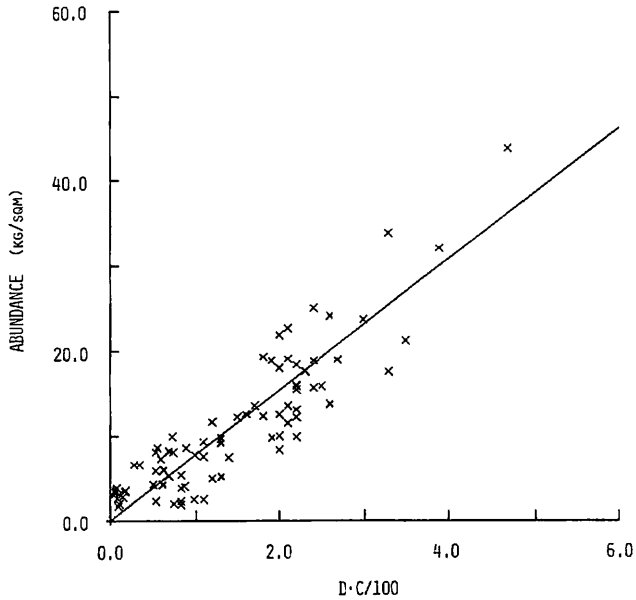

Fig. XIII-4 Relationship between average nodule long axis, nodule coverage and nodule abundance.

The correlation coefficient of the former relation with all measured values except those of V-type nodules is 0.92 and the probable error with the equation (1) is 0.13. The values for the latter equation are 0.75 and 0.37 respectively.

We examined following two methods to estimate nodule abundance from deep-sea photographs: 1) to measure the length of long axis of each nodule existing in a certain area on the photograph and convert it into nodule weight using an equation (1), subsequently to sum them up and to estimate nodule abundance in kg/m^2; 2) to obtain an empirical equation which is related to nodule abundance and nodule coverage, and to estimate nodule abundance from the photograph with this equation.

The relationship between the length of long axis and weight of nodule has already been given as the equation (1). Figure XIII-4, which is obtained by rearranging nodule abundance, nodule coverage and average nodule long axis, shows the relation used in the latter method. The curve in this figure is a linear regression determined by the method of least squares using the data from box corer and freefall photo grab hauls. The equation for the line is:

$$A = 7.7 \times D \times C/100 \quad \text{.....(3)}$$

where A: nodule abundance (kg/m^2)
D: average length of nodule long axis (cm)
C: nodule coverage (%)

The correlation coefficient is 0.89 and the probable error with the equation (3) is 2.5.

Figure XIII-5 shows size and mass distribution of nodules which are sampled at the sampling points where nodule coverage is more than 50% in box cores and in deep-sea photographs. This figure indicates that size frequency of nodules under 1 cm is about 6% and their mass occupies only 0.3% of the whole mass. This suggests that nodules

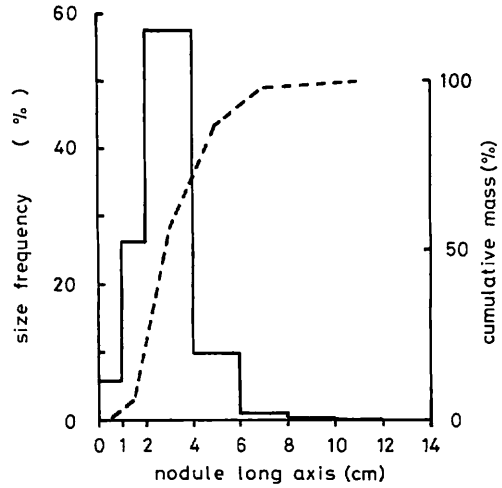

Fig. XIII-5 Size and mass distribution of nodules sampled at sites where nodule coverage are more than 50% in box cores and in deep sea photographs.

under 1 cm in long axis are not significant in estimation of nodule abundance from deep-sea Photographs. However, it is necessary to continue obtaining such data and to study statistical considerations in order to determine the cut-off size fractions as well as to determine the regression equations (1) through (3).

Some results estimated by the above two methods are shown in Table XIII-1. These estimates give good agreement almost within 20% compared to actual nodule abundance which is calculated from the weight of sampled nodules.

Reference

MORITANI, T., MARUYAMA, S., NOHARA, M., KINOSHITA, Y., OGITSU, T., and MORIWAKI, H. (1977) Description, classification and distribution of manganese nodules. *In* MIZUNO, A. and MORITANI, T. (*eds.*), *Geol. Surv. Japan Cruise Rept.*, no. 8, p. 136–158.

Table XIII-1 Some results of estimation of nodule abundance from deep-sea photographs.

FG No.	results of on-site observation: nodule abundance (kg/m²)	nodule coverage (%)	average nodule long axis (cm)	estimates from deep-sea photographs: average nodule long axis (cm)	method* (1) (kg/m²)	method* (2) (kg/m²)	remarks	
FG 122 C–2	(3.2)**	60	3.2	3.4	14.5 (18%)***	15.7 (28%)	FG 122–1	12.1 kg/m²
							C–1	12.3 kg/m²
							–2	12.5 kg/m²
FG 127 C–1	24.1	80	3.3	3.6	22.6 (− 6%)	22.2 (− 8%)		
FG 127 C–2	22.7	80	3.0	3.5	19.0 (−16%)	21.6 (− 5%)		
FG 128 C–2	(7.8)	85	3.6	4.2	21.0	27.5	FG 128–1	32.1 kg/m²
							C–1	33.9 kg/m²
							–2	21.3 kg/m²
FG 148 C–1	18.0	60	3.3	3.2	14.9 (−17%)	14.8 (−18%)	FG 148C–2	12.6 kg/m²
FG 153 C–1	18.9	55	3.4	3.5	15.4 (−19%)	14.8 (−22%)		
FG 153 C–2	19.3	55	3.3	3.9	16.5 (−15%)	16.5 (−15%)		
FG 160 C–1	17.6	80	4.1	3.7	20.5 (16%)	22.8 (30%)		
FG 160 C–2	23.7	80	3.7	3.6	22.4 (− 5%)	22.2 (− 6%)		
FG 161 C–1	(0.0)	80	–	4.6	26.8	28.3	G(B) 953	43.8 kg/m²
FG 162 C–2	(8.9)	75	3.0	3.2	19.4 (24%)	18.5 (18%)	FG 162C–1	15.7 kg/m²
FG 164 C–1	(7.2)	80	3.4	2.7	15.5	16.6	FG 164C–2	(2.2 kg/m²)

(note) *see the text, method (1) is based on the equation (1) and method (2) is on the equation (3).

**nodule abundance in parantheses shows probably incorrect values due to imperfect sampling, judged from sea bottom photograph data by freefall photo grab sampler.

***agreement shown in percent is calculated by following equation:

$$\text{agreement}(\%) = \left(\frac{\text{calculated value}}{\text{actual value}} - 1\right) \times 100$$